Wideband Beam-Switchable 28 GHz Quasi-Yagi Array for Mobile Devices

Paola, Carla di; Zhang, Shuai; Zhao, Kun; Ying, Zhinong; Bolin, Thomas; Pedersen, Gert Frølund

Published in:
I E E E Transactions on Antennas and Propagation

DOI (link to publication from Publisher):
10.1109/TAP.2019.2925189

Publication date:
2019

Document Version
Accepted author manuscript, peer reviewed version

This article has been accepted for publication in a future issue of this journal, but has not been fully edited. Content may change prior to final publication. Citation information: DOI 10.1109/TAP.2019.2925189, IEEE Transactions on Antennas and Propagation

Wideband Beam-Switchable 28 GHz Quasi-Yagi Array for Mobile Devices

Carla Di Paola, *Student Member, IEEE*, Shuai Zhang, *Senior Member, IEEE*, Kun Zhao, Ying Zhinong, *Senior Member, IEEE*, Thomas Bolin, Gert Frølund Pedersen, *Senior Member, IEEE*

***Abstract*—The goal of this paper is to propose a new antenna array architecture, that aims to solve the most known limitations of phased antenna arrays, resulting a good candidate for next 5G mobile handsets. The architecture consists of five Quasi-Yagi antennas printed on the short edge of a Roger RO3003 substrate, pointing different directions, and a switch to feed each antenna and steer the beam. Simulations prove that the antenna array can cover the angle of over 180° with high gain over the frequency range from 26 to 40 GHz. Alternative designs to make the structure more compact further demonstrate the validity of the concept. The optimized corner array of four elements is fabricated and passive and active measurements are performed with the MVG Starlab 50 GHz. The results of the passive measurements are in accordance with the simulations and show that the proposed Quasi-Yagi antenna array has large coverage over the whole bandwidth and peak gain of 8 dBi at 28 and 38 GHz. The active measurements of the array connected to the FEM and integrated in the phone-case further confirm the radiation properties of the switchable antenna array at 28 GHz in a quasi-real scenario.**

***Index Terms*—Mobile terminal antennas, directional antennas, multibeam antenna array, high gain, wideband, 28 GHz.**

I. Introduction

THE centimeter/millimeter wave bands provide wide bandwidths that can support the higher data rates required by the future 5G applications [1]. However, by increasing the operating frequency, the signal wavelength becomes shorter and consequently the free-space path loss is higher, according to the Friis transmission equation [2], [3]. Thus, higher gain antennas are needed to compensate the large path loss [4]. Since high gain leads to narrow radiation beamwidth, the existing phased arrays are also required to reach a large beam steering range. Phased antenna arrays present though bandwidth limitations, since phase shifters do not provide the correct rate of change of phase with frequency, to guarantee the same beam pointing over a wide bandwidth [5]–[7]. Also the chosen array element distance is constrained by the frequency, that influences the gain at the lowest frequency and the coverage at the highest frequency of the interval. Moreover, due to the limited space reserved in mobile handsets to place the antenna, the design of compact phased arrays becomes extremely challenging.

For example, the quad-element microstrip patch antenna array proposed in [8], achieves a realized gain of 13.5 dBi at 28 GHz, but presents a complicated layered structure and is placed in a clearance of 10 mm width. In [9], to obtain 3D-coverage with high gain at 28 GHz, three subarrays of slot antennas are employed to switch their beam to three distinct regions. The design aims to overcome the limitations of directional-phased arrays [10], exploiting the switching characteristic of the antenna to achieve three-dimensional scanning coverage, but requires a significant portion of PCB. The same strategy is adopted for the three subarrays of microstrip patch antennas introduced in [11]. The structure occupies, though, the whole upper part of the mobile phone PCB. Moreover, the above mentioned phased antenna arrays have a limited bandwidth, e.g. only 1 GHz for the last case. A wider bandwidth of 3.6 GHz characterizes the four eight-element subarrays described in [12]. To obtain spherical coverage, two subarrays have been positioned orthogonally to the top and bottom edges of the PCB, making though the structure difficult to fabricate. On the contrary, the phased array of slot antennas arranged on the upper frame of the metal-body of the mobile handset in [13] presents simple architecture and space optimization, reaching a gain of 13.7 dBi at 28 GHz. However, the bandwidth is limited to 1.5 GHz. The efforts in [14] allow the realization of a dual band phased antenna array at 28 and 38 GHz, despite the complicated structure and the amount of space occupied on the PCB. By contrast, a simple design is presented in [15], but the Quasi-Yagi antenna generates only a unidirectional pattern in the endfire direction with low realized gain of 6.5 dBi. Yagi-Uda and Qausi-Yagi antenna are also chosen for the phased array and the switchable array in [16], [17]. Other end-fire type phased arrays are proposed in [18]–[20]. In particular, in [19] the Vivaldi antenna exhibit high gain of 15.9 dBi and the 8-element array in [20] achieves a scan angle of over 140° with realized gain of 13 dBi on average over the 8 GHz bandwidth.

The multilayer structure of the beamforming network featuring the substrate integrated lens aims to obtain size reduction and guarantees low profile, low cost and high performance. On the other hand, this component suffers from narrow band and high loss, as confirmed by the research works in [21]–[24].

A compact layered topology characterizes also the beam-

This work was supported by the InnovationsFonden project of Reconfigurable Arrays for Next Generation Efficiency (RANGE). (Corresponding author: Shuai Zhang).

Carla Di Paola, Shuai Zhang and Gert Frølund Pedersen are with the Antennas, Propagation and mm-Wave Systems (APMS) section at the Department of Electronic Systems, Aalborg University, Denmark (email: {cdp, sz, gfp}@es.aau.dk).

Kun Zhao, Ying Zhinong and Thomas Bolin are with the Corporate Technology Office, Sony Mobile Communication AB, Lund, Sweden (email: {Kun.X.Zhao, Ying.Zhinong, Thomas.Bolin}@sony.com).

Kun Zhao is also with the Antennas, Propagation and mm-Wave Systems (APMS) section at the Department of Electronic Systems, Aalborg University, Denmark.

This article has been accepted for publication in a future issue of this journal, but has not been fully edited. Content may change prior to final publication. Citation information: DOI 10.1109/TAP.2019.2925189, IEEE Transactions on Antennas and Propagation

forming network based on a Butler matrix [25]–[27]. Giving the advantage of covering a wider bandwidth, this kind of feeding network is affected, though, by higher loss than lens.

The novelty of the proposed design is the realization of a wideband antenna array, with large coverage and high-gain at all the frequencies. The architecture includes five high gain antennas, placed in the upper edge of the mobile device, realized by optimization of a microstrip-fed Quasi-Yagi antenna. The antennas do not require phase shifters to steer the beam and obtain the coverage but, by simply switching the feeding to one of the elements, it is possible to scan the desired areas. Therefore, the configuration allows to solve the bandwidth limitations of the most common phased antenna array, suppressing any constraint on the phase, that guarantees the main beam direction in a wide frequency range. Moreover, due to the absence of any constraint in the distance between adjacent elements, the antennas are placed in such a way that ensures low mutual coupling and reduces the spurious lobes that affect the radiation pattern [28].

On the other hand, the switchable antenna system results though in a physically larger setup, since only one antenna is used at a time, compared to the phased array, that allows to save in antenna area, as the whole aperture is always exploited. Other drawbacks are the absence of the array multiplication factor and the smaller number of available discrete beams responsible of more dips in the envelope, as opposed to phased arrays which can steer the beam smoothly, providing higher gain across the scanning range. Last but not least, the proposed solution is less flexible compared to phased arrays, where the possibility to select different phase shifts allows to generate several beams. However, while it is still extremely challenging for a phased antenna array to achieve a scanning angle larger than $-/+60^\circ$ with an acceptable beam quality [29], the switchable antenna array has been demonstrated to reach a range coverage wider than $-/+90^\circ$ and, if placed also at the bottom of the mobile phone, allows to cover the other half of the space.

Finally, comparing the proposed structure with the equivalent phased antenna array in Fig. 1, where a phase controller is needed for the input signal of every antenna, only a switch is used in order to feed the antenna that covers the corresponding area.

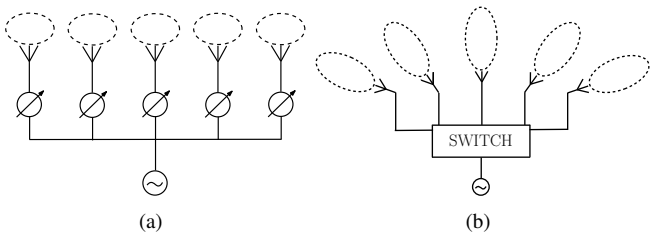

Fig. 1. Sketch of (a) a phased array of 5 elements and (b) the proposed switchable array of 5 antennas.

The paper is organized as follows. The design of the structure is presented in Section II, along with the analysis conducted on the simulated prototype. Section III illustrates alternative placements and optimizations of the antenna system. Section IV shows the results of the passive measurements run on the realized component, followed by a comparison with the results obtained from the simulations. Section V deals with the phone house integration impact evaluated through active measurements. Finally, Section VI concludes the paper.

II. Quasi-Yagi antenna array

A. Antennas configurations

The proposed package, shown in Fig. 2, presents a symmetric structure consisting of five mictrostrip fed Quasi-Yagi antennas. Yagi-Uda antennas have been chosen to obtain unidirectional radiation and high gain, due to their simple structure, small size, ease of fabrication and low cost [30], [31]. In order to steer the beam of 180°, each antenna should ideally have 36° beamwidth, scanning different parts of the space. To achieve the desired coverage, the original antenna has been bended by 75°, giving the first and symmetrically the fifth antenna, pointing respectively to the left and right side of the area. For the second and fourth antenna, it had to be bent 35°, in order to cover the upper left and right part of the space. Finally, the original antenna pointing 90° allows to scan the top of the sphere. In this way, the properties of wide band and large coverage can be realized by a simple switchable system of different antennas.

The antennas are built on both sides of a Rogers RO3003 substrate with permittivity $\epsilon_r = 3$ and loss tangent $tan\delta = 0.001$. The substrate has the length of 130 mm, width of 70 mm and thickness of 0.762 mm. Antennas dimensions are listed in Table I. The truncated ground plane acts as reflector to maximize the antenna gain. Concerning the bended ground plane, it is designed following the same inclination as the corresponding antenna, in order to focus the energy in the endfire direction. The driving dipoles are printed symmetrically on both faces of the substrate. In particular, half dipole, placed in the bottom of the structure, is grounded in the antenna ground plane and half dipole on top is connected to a microstrip line fed by an SPMS connector. The number of directors of the three central antennas has been reduced, to minimize the length of the clearance to 6.5 mm. The directors are printed on both sides of the substrate in order to maximize the beam directivity. The ladder-like directors, proposed in [32] for antenna gain and bandwidth enhancement, are chosen for the central and the corner antennas. Compared to a single director, multidirectors provide a spatial wave combination and further enhance the wave propagation in the endfire direction. The three central antennas present a bowtie driver, that allows to improve the bandwidth [33], [34]. In fact, the bowtie antenna, unlike the half-wavelength dipole, is specified by the angle of the equilateral triangles, not by the length, and hence is frequency independent. Two symmetric extended stubs have been added in order to confine their beam, enhancing thus the directivity.

The main goal of the design is the realization of an antenna array that achieves a scan angle of 180° within a wide band by simply switching to the feed of one element at a time. Then the positive results obtained from both simulations and measurements of the realized component encouraged the authors to test the performance of the prototype directly in the

This article has been accepted for publication in a future issue of this journal, but has not been fully edited. Content may change prior to final publication. Citation information: DOI 10.1109/TAP.2019.2925189, IEEE Transactions on Antennas and Propagation

real scenario, where the antenna array is integrated in a phone case with a glass.

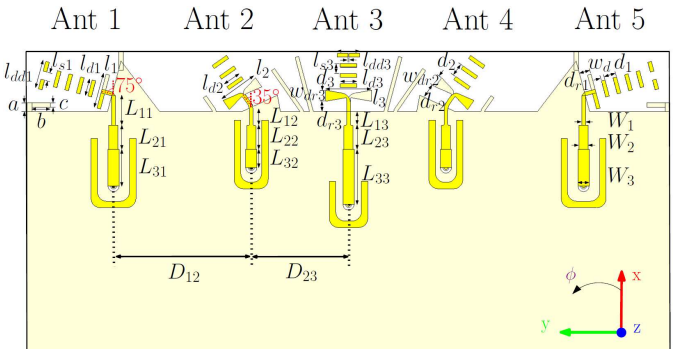

Fig. 2. Geometric structure and parameters of the proposed planar printed Quasi-Yagi antennas for 5G mobile-phones.

TABLE I
DIMENSIONS OF THE 5G ANTENNAS PARAMETERS (UNITS: MM).

Parameter	Value	Parameter	Value	Parameter	Value
D_{12}	15	W_1	0.4	l_2	4.3
D_{23}	10.6	W_2	1	l_{d2}	1.9
L_{11}	3.2	W_3	1.2	w_{dr2}	1.2
L_{21}	2.6	a	0.95	d_2	1.4
L_{31}	4	b	2	d_{r2}	1.7
L_{12}	1.6	c	0.5	l_3	5
L_{22}	2.5	l_1	3.8	l_{d3}	1.8
L_{32}	2	l_{d1}	1.8	l_{dd3}	2.44
L_{13}	1.4	l_{dd1}	3.08	l_{s3}	0.1
L_{23}	2.5	l_{s1}	0.92	w_{dr3}	1.2
L_{33}	6	d_1	1.3	d_3	1.1
w_d	0.4	d_{r1}	1.2	d_{r3}	1.1

B. Antennas' performance

The structure has been analyzed using the electromagnetic simulator *CST Microwave Studio 2018*. The curves reproduced in Fig. 3(a) represent the S-parameter characteristics of the proposed design. Each Yagi-Uda antenna presents wide band, allowing the whole system a -10 dB matching bandwidth from 26 to 40 GHz. The presence of resonant frequency points in the reflection coefficient of each Yagi-Uda antenna is due to the concentration of the current along the driving dipoles. The port-to-port isolation between the neighboring elements is over 20 dB, as proved in Fig. 3(b). Fig. 3(c) highlights that the realized gain of each component, is above 7 dBi over the -10 dB impedance bandwidth of $26 - 40$ GHz. With no more than 15.4 dBm input power to the antenna, it can meet the requirements on EIRP approved by the *3GPP* standard [35]. Moreover, the averaged gain at 28 GHz is about 8 dBi and 9 dBi at 38 GHz. The values in Fig. 3(c) represent the maximum gain evaluated in the direction of the main lobe, which varies with the frequency. Table II reports this direction for antenna 1, 2 and 3 at 28 and 38 GHz (antenna 4 and 5 are symmetrical to 2 and 1 respectively). Considering that the difference is around 8° on average and the main lobe calculated for each antenna element at the other frequency points of the -10 dB bandwidth follows approximately the same direction, it is possible to state that the radiation pattern is overall stable.

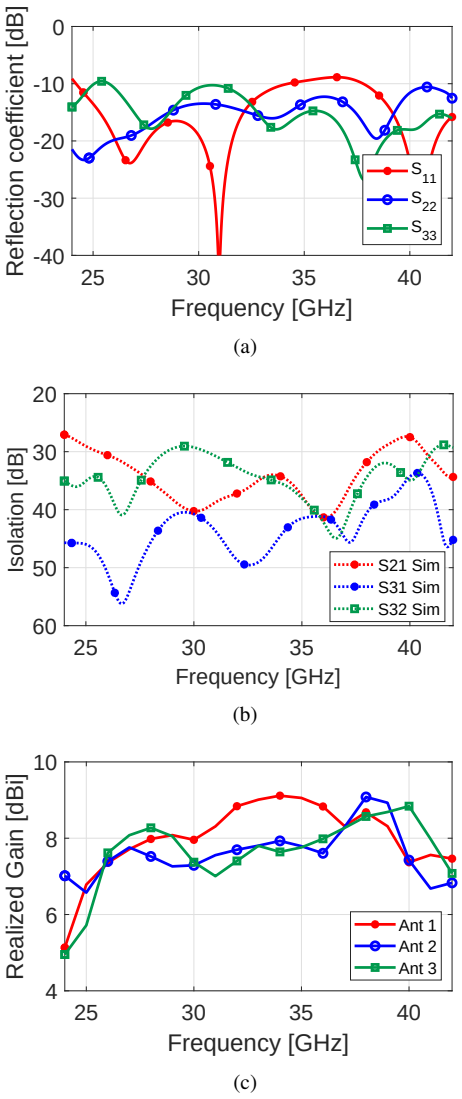

Fig. 3. Simulated S-parameter characteristics of the proposed antenna package, (a) return loss and (b) port-to-port isolation, and (c) realized gain of each Yagi-Uda antenna element. Due to the symmetric structure, the S-parameter and gain of antennas 4 and 5 are omitted here.

TABLE II
MAIN LOBE DIRECTION OF ANTENNA 1, 2 AND 3 AT 28 AND 38 GHZ.

Antenna	28 GHz	38 GHz
1	71°	81°
2	38°	43°
3	−4°	5°

Figure 4 shows the 3D radiation characteristic of the antenna system at 28 GHz. It is possible to verify that the radiation pattern of the first and fifth antennas are symmetric and the same applies to the second and fourth antennas. As expected, each antenna covers a specific portion of the sphere with high gain. Therefore, in order to scan the desired area, it is necessary to switch to the feed of the corresponding antenna.

This article has been accepted for publication in a future issue of this journal, but has not been fully edited. Content may change prior to final publication. Citation information: DOI 10.1109/TAP.2019.2925189, IEEE Transactions on Antennas and Propagation

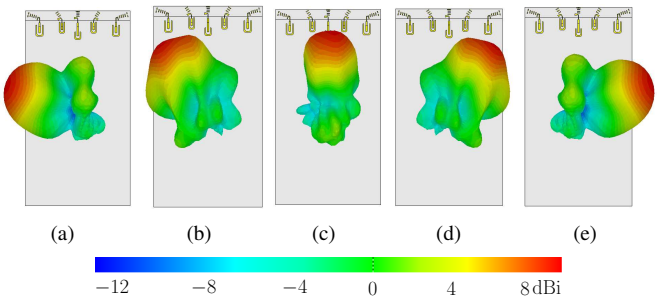

Fig. 4. Placement of the 28 GHz Yagi-Uda antenna (a) 1, (b) 2, (c) 3, (d) 4 and (e) 5 within the edge regions of the 5G cellular handset and their desired coverage.

The radiation patterns depicted in Fig. 5 represent the coverage of the antenna package at 38 GHz. It is possible to notice a partial overlap of the patterns, that allows to increase the gain in the pointed area. Moving to the upper part of the bandwidth, the beamwidth is expected to be narrower and the gain consequently higher.

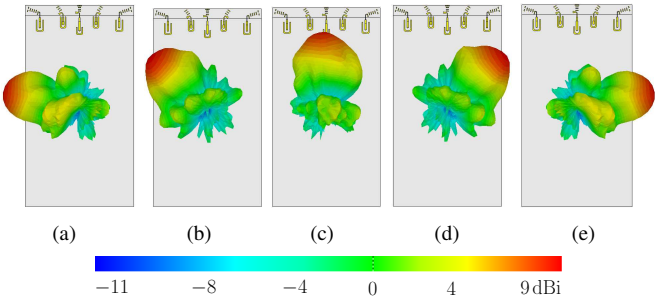

Fig. 5. Simulated radiation patterns of the antenna element (a) 1, (b) 2, (c) 3, (d) 4 and (e) 5 at 38 GHz.

The 2D-coverage property of the antennas system for the selected frequencies is reported in Fig. 6. The curve representing the envelope at 28 GHz shows that it is possible to cover an area of 180° with a maximum gain of 8.2 dBi and minimum of 6.2 dBi. However, the ripple of 2 dB is negligible, as the requirements of the *3GPP* standard [35] concern the peak EIRP/gain and allow a maximum difference of 10.9 dB below the peak EIRP/gain within the covered solid angle. In particular, each antenna is able to steer 40° beamwidth on average, with peak gain at 71°, 38° and −4° respectively for the first, second and third element, and symmetrically at −37° and −71° for the fourth and fifth. From the comparison with the plot reproducing the coverage at 38 GHz, it is possible to notice that the beamwidth of each element is slightly narrower, with consequently higher ripple of 3.5 dB, as expected, between the peak gain of 9 dBi and minimum gain of 5.5 dBi.

III. Alternative Designs

The flexibility of the proposed antenna system allows to deploy different topologies and locations in a mobile handset. Therefore, in order to optimize the space occupied by the array, alternative placements are arranged.

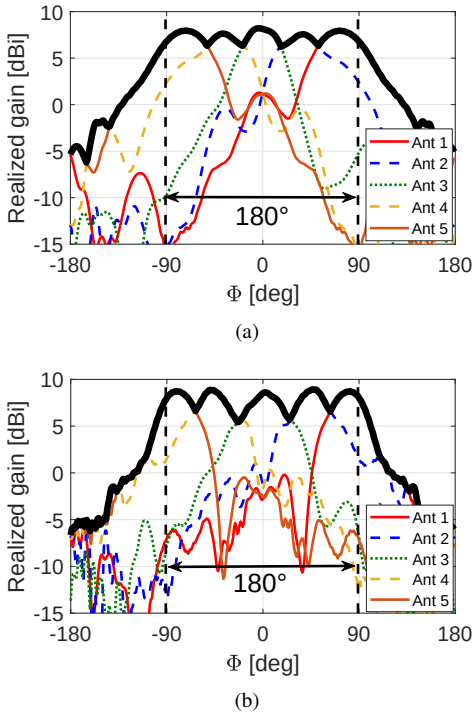

Fig. 6. Spherical coverage of the 5-element antenna system at (a) 28 GHz and (b) 38 GHz.

A. Side placement

The first step focuses in reducing the distance between the elements to $\lambda/2$ and moving the new compact antenna system to the left side of the PCB, breaking thus the symmetry of the structure (Fig. 7). A wide portion of clearance, $d = 10$ mm, has been saved to allocate to other components of the mobile device. This new positioning required, though, to adjust the length of the microstrip feeding lines, to improve impedance matching. Therefore, L_{31} has been extended to 6.5 mm and L_{33} is 2.6 mm longer. The aim of the new design is to exploit the neighboring antennas as passive elements, with the only function to direct the beam towards the desired direction. In fact, comparing the curves in Fig 8, the presence of antenna 1 and 3 is fundamental for antenna 2 to point the main beam to 30° instead of 60°. The gain is also 1.3 dB higher thanks to the neighboring elements. The −10 dB impedance bandwidth covers $24 - 42$ GHz with port-to-port isolation higher than 20 dB. Fig. 9(a) shows that the realized gain of each component is higher than 6 dBi in the band $28-42$ GHz. In Table III the direction of the main lobe for each antenna element is given at the reference frequency points, 28 and 38 GHz. As depicted in Fig. 9(b), a broader coverage with a scanning angle wider than 180° is guaranteed. Due to the asymmetry, the first and fifth antenna have different radiation pattern and gain. In particular, the gain of the fifth element decreases 1.5 dB compared to the case of placing this array in the middle of the short edge. Moreover, the three central antennas suffer a decrease in gain of 1 dBi on average, because of the smaller distance between each other. Therefore, the side configuration achieves maximum gain of 7.7 dBi and

This article has been accepted for publication in a future issue of this journal, but has not been fully edited. Content may change prior to final publication. Citation information: DOI 10.1109/TAP.2019.2925189, IEEE Transactions on Antennas and Propagation

minimum of 4.2 dBi, giving thus a ripple of 3.5 dB.

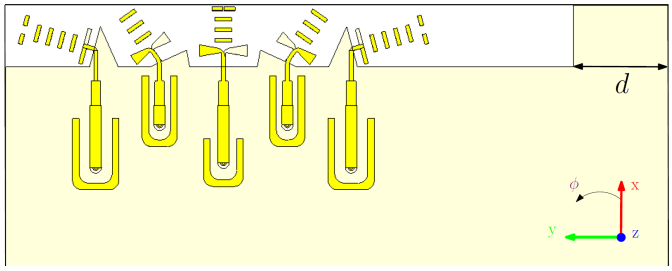

Fig. 7. Side placement of the Yagi-Uda antenna package.

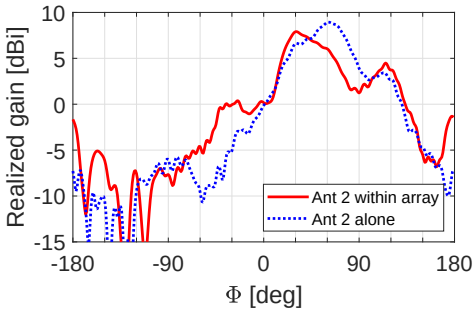

Fig. 8. 2D radiation pattern of antenna 2 with and without the presence of the antenna 1 and 3 as passive elements.

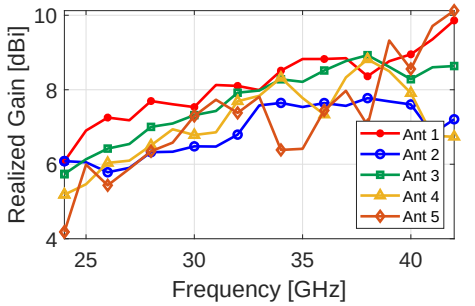

(a)

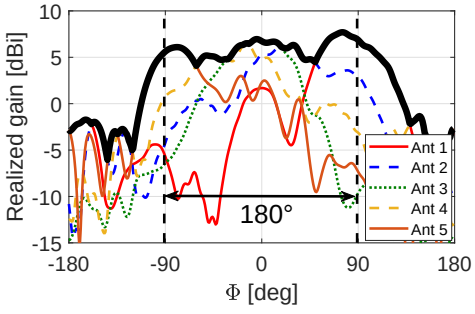

(b)

Fig. 9. (a) Realized gain of each Yagi-Uda antenna element in the side placement as a function of the frequency and (b) spherical coverage at 28 GHz.

B. Corner placement

In order to make the structure more compact and occupy a smaller area on the PCB, the Yagi-Uda antennas have been positioned in the corner (Fig. 10). In the new location only four antennas are required to guarantee the same coverage but, unlike the previous configurations, the corner placement allows to cover the right side of the sphere, instead of the upper part. A distance $D_{12} = 6.25$ mm divides the two antennas on top, whereas the other two elements in the side are placed $D_{34} = 7$ mm apart. The antenna system is located $d_1 = 48$ mm distant from the left side and $d_2 = 75$ mm from the bottom. The -10 dB impedance bandwidth is $24-42$ GHz with port-to-port isolation higher than 20 dB. Fig. 11 shows that the realized gain of each component is higher than 7 dBi in the band $28 - 40$ GHz. As for the previous designs, the direction of the main lobe for each antenna element at 28 and 38 GHz is reported in Table IV. In this case, even though the direction of the radiation pattern is not stable over the frequency interval, the desired scan angle is obtained, because the main lobe of each antenna results rotated of approximately the same angle. Finally, the same structure, printed in the opposite corner, guarantees to cover the total sphere. For all the afore-mentioned advantages, the authors decided to fabricate the corner antenna array system, which represents a good trade-off between performances and dimensions.

TABLE III
MAIN LOBE DIRECTION OF THE ANTENNA ELEMENTS AT 28 AND 38 GHZ.

Antenna	28 GHz	38 GHz
1	75°	78°
2	29°	31°
3	−5°	0°
4	−14°	−36°
5	−79°	−92°

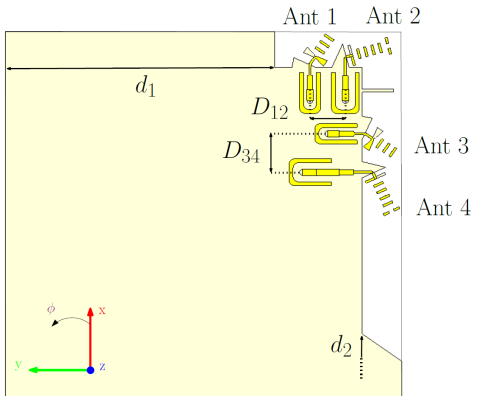

Fig. 10. Corner placement of the Yagi-Uda antenna package.

TABLE IV
MAIN LOBE DIRECTION OF THE ANTENNA ELEMENTS AT 28 AND 38 GHZ.

Antenna	28 GHz	38 GHz
1	−19°	−37°
2	−45°	−77°
3	−110°	−127°
4	−147°	−167°

This article has been accepted for publication in a future issue of this journal, but has not been fully edited. Content may change prior to final publication. Citation information: DOI 10.1109/TAP.2019.2925189, IEEE Transactions on Antennas and Propagation

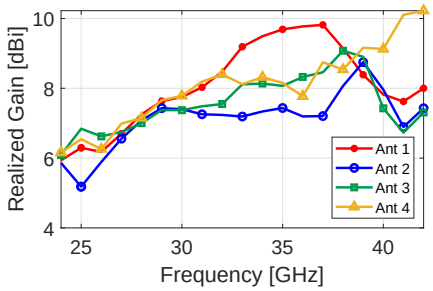

Fig. 11. Realized gain of each Yagi-Uda antenna element in the corner placement as a function of the frequency.

IV. Passive Measurements Results and Discussion

Figure 12(a) is the photograph of the fabricated corner Yagi-Uda array prototype. S-parameters are evaluated using the Keysight N5227A Power Network Analyzer (PNA) and are presented in Fig. 13 for comparison with the corresponding simulation results. The curves related to the return loss of the realized component show a higher value of the reflection coefficient, but the -6 dB bandwidth is confirmed to be $26-40$ GHz. Same considerations apply to the measured insertion loss for all the ports, which is less than -20 dB, reporting a good agreement between simulations and measurements.

Figure 12(b) shows the setup for the passive measurements, carried out in the frequency interval $26-40$ GHz. The radiation performance of the realized component have been measured with the MVG Starlab 50 GHz in Paris. A description of both passive measurements run over the antenna mockup followed by active measurements conducted on the array integrated into the phone-case is given along with the corresponding results.

In particular, the simulated and measured radiation pattern cuts at $\theta = 90°$, calculated both at 28 and 38 GHz (Fig. 14 and Fig. 15 respectively), prove that the desired beam scanning of $180°$ is achieved. Moreover, the curves follow the same trend but, at the lower frequency point, the realized component suffers a decrease in gain of around 1 dB and a higher ripple compared to the simulations. In fact, the measured peak gain is 6.5 dBi, versus the simulated of 7.8 dBi, and the minimum gain drops from 4.2 dBi in simulations, where the ripple is 3.4 dB, to 1 dBi in measurements, giving thus a ripple of 5.5 dB. A better agreement is shown at 38 GHz, with measured maximum and minimum gain of 9.6 and 1.6 dBi respectively and consequent higher ripple than 28 GHz, as expected.

Fig. 16 reports the comparison between the 3D radiation patterns at 28 GHz, which represent the total power at both polarizations. The measurement setup allowed to evaluate the realized gain of the four Yagi-Uda antenna for each value of ϕ while θ varies from $0°$ to $180°$. The measured radiation patterns in Fig. 16(b) match the ones obtained from the simulations in Fig. 16(a). The antennas cover the proper area, even though with lower gain, which decreases significantly for $\theta > 160°$, due to limitations of the measurements setup. Same considerations apply to the simulated and measured 3D radiation pattern at 38 GHz, showed in Fig. 17. The plots highlight also that the measured gain is approximately 2 dB

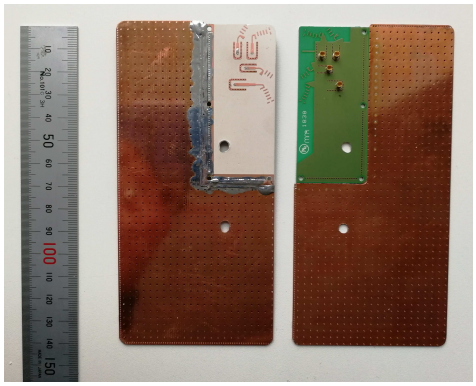

(a)

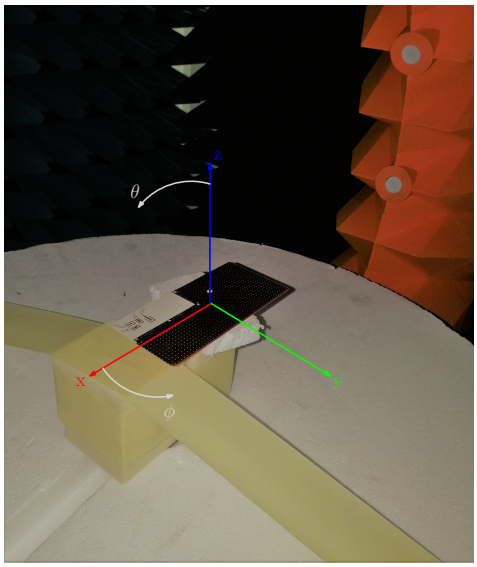

(b)

Fig. 12. Fabricated Yagi–Uda antennas on a Rogers RO3003 substrate (top and bottom layer) and passive measurements setup in the MVG StarLab 50 GHz.

higher compared to the lower frequency and, as expected, the beamwidth is narrower both along ϕ and θ.

Looking at the plots of the total scan pattern (TSP) in Fig. 18, it is possible to state that the expected beam steering of $180°$ is obtained. The TSP of an antenna array is obtained from all array patterns corresponding to the beam for the different array scan angles by extracting the best achievable gain value at every angular distribution point. In other words, the TSP of this design is the 3D envelope of all the individual antenna patterns. The spatial performance of the antenna array can be evaluated in terms of the coverage efficiency [36]:

$$\eta_c = \frac{\text{Coverage Solid Angle}}{\text{Maximum Solid Angle}} \tag{1}$$

where maximum solid angle is defined as 4π steradians in order to account for the arbitrary angle of arrival and arbitrary orientation of the mobile device. The coverage efficiency is calculated from the total scan pattern with respect to the chosen set of the gain values.

This article has been accepted for publication in a future issue of this journal, but has not been fully edited. Content may change prior to final publication. Citation information: DOI 10.1109/TAP.2019.2925189, IEEE Transactions on Antennas and Propagation

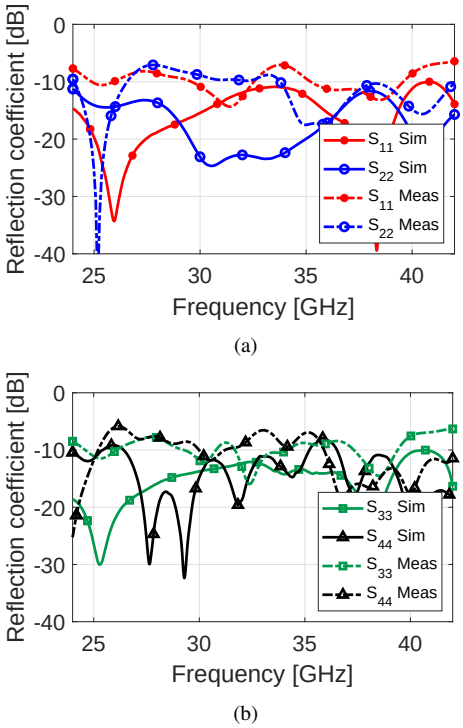

Fig. 13. Comparison of the simulated and measured S-parameter characteristics of (a) array elements 1 and 2, and (b) antenna 3 and 4.

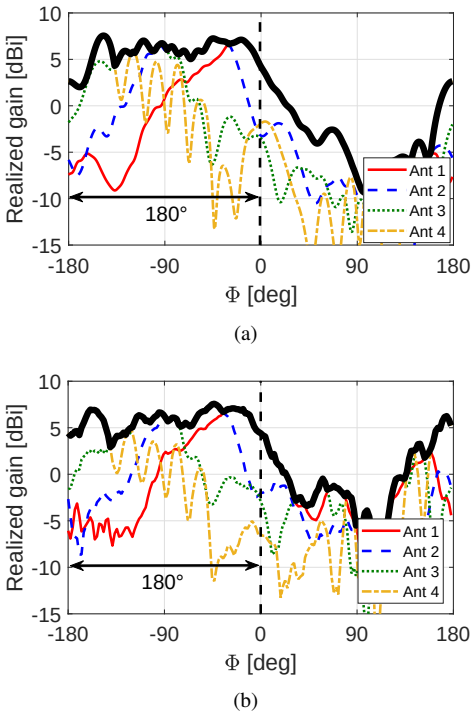

Fig. 14. 2D-radiation pattern evaluated at $\theta = 90°$ of the of the (a) simulated and (b) measured antennas package at 28 GHz.

In Fig. 19 the coverage efficiency at 28 and 38 GHz is plotted versus the realized gain. Fixed $\eta_c = 0.5$, the gain of the measured structure at 28 GHz is approximately 3 dB lower than the simulated one. From the comparison of the curves representing the coverage efficiency at the higher

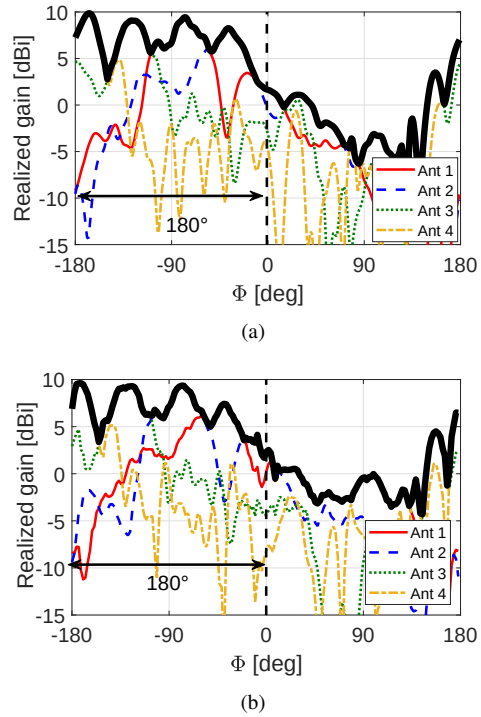

Fig. 15. 2D-radiation pattern evaluated at $\theta = 90°$ of the of the (a) simulated and (b) measured antennas package at 38 GHz.

frequency, it is possible to notice a reduction in gain of 2 dB in the measurements, compared to the simulations. The significant decrease in gain performance can be justified by the poorer matching of the realized component compared to the simulations, that can be caused by the installation of the connectors as well as the antenna mockup fabrication issues.

V. Active Measurements and Phone House Integration Impact

This section investigates the activate front end module (FEM) and phone house integration impact on the antenna array performance, in order to validate its feasibility for mobile handset application. The active measurements are performed on the Yagi-Uda antenna array, connected to the FEM and placed inside a polycarbonate case, 0.7 mm distant from the cover. The dimensions are given in Fig 20(b). The main parts of the FEM, realized by Sony, are highlighted in Fig. 20(a). It is composed by a Power Amplifier (PA), a Low Noise Amplifier (LNA) and two single-pole, four-throw (SP4T) switches. The first SP4T swtich is used for swithcing between PA and LNA and the second SP4T switch is for selecting the active element. The LNA is open during the measurements, since the performance are evaluated only in the transmission phase. The gain characteristic of the FEM evaluated in the frequency band $20 - 40$ GHz is plotted in Fig. 21(b), along with a picture of the measurement setup in Fig. 21(a), and highlights 15 dB gain at 28 GHz. Moreover, Table V contains the information regarding the feeding network and the gain of the antenna elements at the measured frequency point for the calculation of the link budget. The active measurements setup, shown in Fig. 20(c), consists of a spectrum analyzer connected

This article has been accepted for publication in a future issue of this journal, but has not been fully edited. Content may change prior to final publication. Citation information: DOI 10.1109/TAP.2019.2925189, IEEE Transactions on Antennas and Propagation

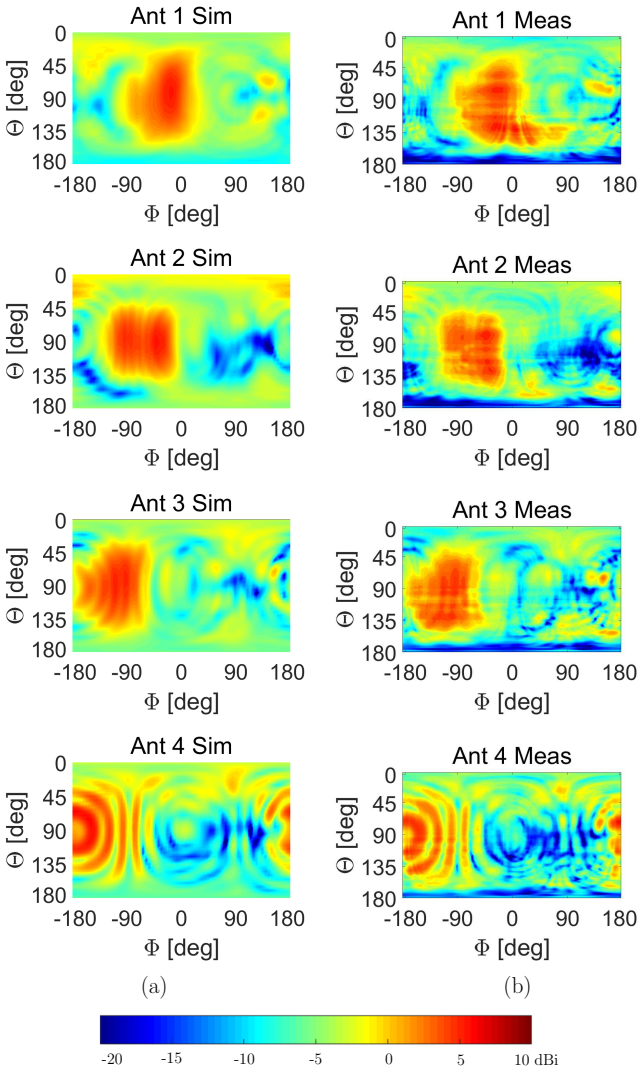

Fig. 16. 3D-radiation pattern (a) simulated and (b) measured at 28 GHz. For ϕ varying from $-180°$ to $180°$ the corresponding value along θ has been plotted.

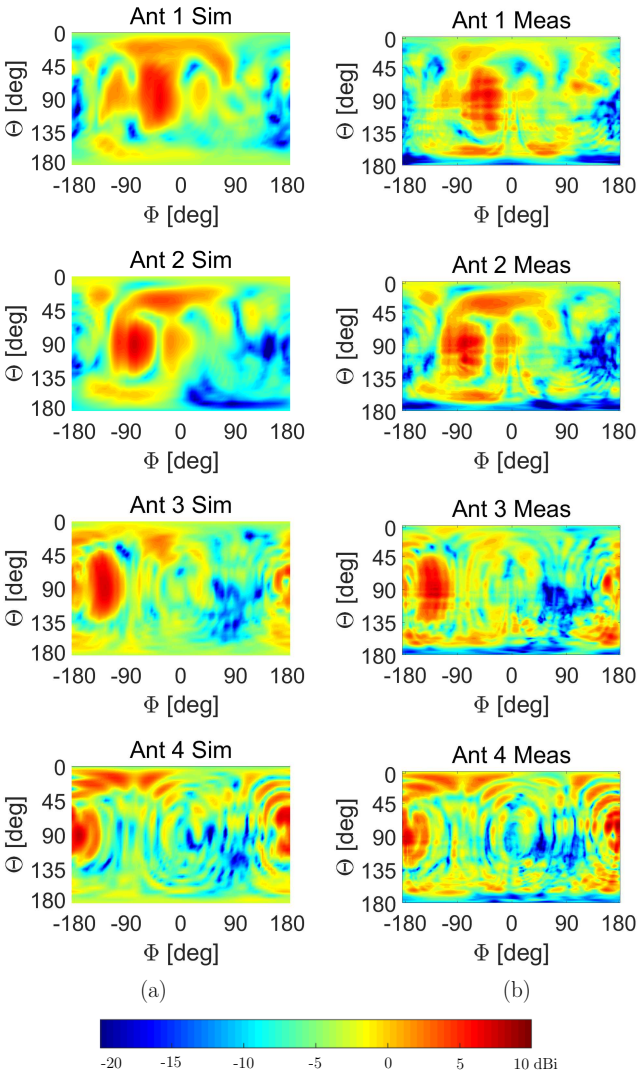

Fig. 17. 3D-radiation pattern (a) simulated and (b) measured at 38 GHz. For ϕ varying from $-180°$ to $180°$ the corresponding value along θ has been plotted.

to the probe array, a power supplier, a signal generator with -10 dBm input power and the power amplifier belonging to the FEM. The 3D-radiation pattern of the four Yagi-Uda antennas, calculated only at 28 GHz, is obtained rotating the setup along ϕ, while θ varies from $0°$ to $162°$.

TABLE V
FEEDING NETWORK AND ANTENNA CHARACTERISTICS AT 28 GHZ FOR THE LINK BUDGET.

Switch	Insertion-Loss = 1.6 dB
FEM	Gain = $14 - 15$ dB *
Cables	Insertion-Loss = 1 dB
Antenna 1	Gain = 8 dB
Antenna 2	Gain = 7.6 dB
Antenna 3	Gain = 7.1 dB
Antenna 4	Gain = 7.8 dB

* The value of the gain of the FEM includes the insertion loss of the switch.

The radiation pattern of each antenna is presented in Fig. 23(a). The desired coverage is achieved at 28 GHz with EIRP of 16.7 dBm on average, due to limitations of the measurement system, which allows only the above mentioned -10 dBm input power. Moreover, an unwanted back radiation caused by the FEM can be observed, though, in the bottom right corner of all the plots, showing a magnitude of 19.5 dBm on average. The responsibility of the FEM for the alteration of the radiation pattern is further proved by the radiation pattern obtained from the simulations (Fig. 22(a)), where the FEM is not included, and is possibly due to the large size of the board and the absence of a shielding structure.

A notable alteration of the radiation properties of the antennas can be attributed to the presence of the display, a glass panel 0.5 mm thick, with permittivity $\epsilon_r = 6$ and loss tangent $\delta = 0.03$. The highly conductive material is responsible for interacting with the electric currents on the surface of the antenna, lowering as a result its performance. In fact, as depicted in Fig. 23(b), each antenna element suffers from a significant decrease in gain, when the glass is mounted on the phone-case. In particular, it is possible to notice that,

This article has been accepted for publication in a future issue of this journal, but has not been fully edited. Content may change prior to final publication. Citation information: DOI 10.1109/TAP.2019.2925189, IEEE Transactions on Antennas and Propagation

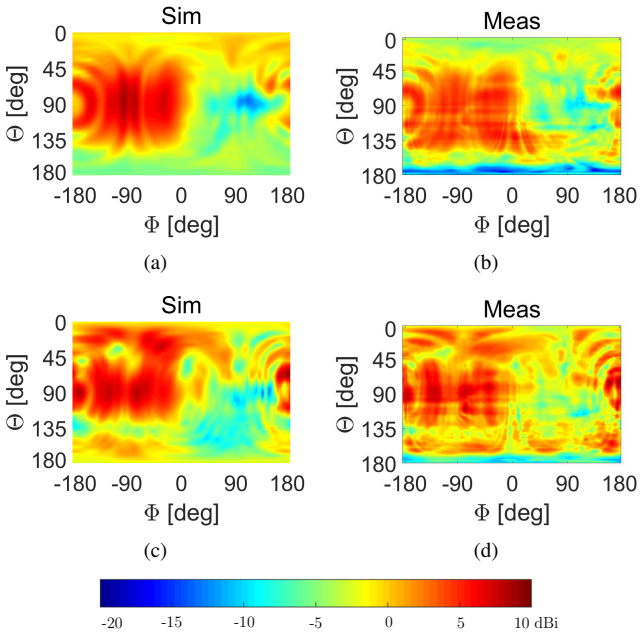

Fig. 18. Total Scan Pattern (TSP) of the proposed antennas package. (a) Simulated and (b) measured at 28 GHz, (c) simulated and (d) measured at 38 GHz.

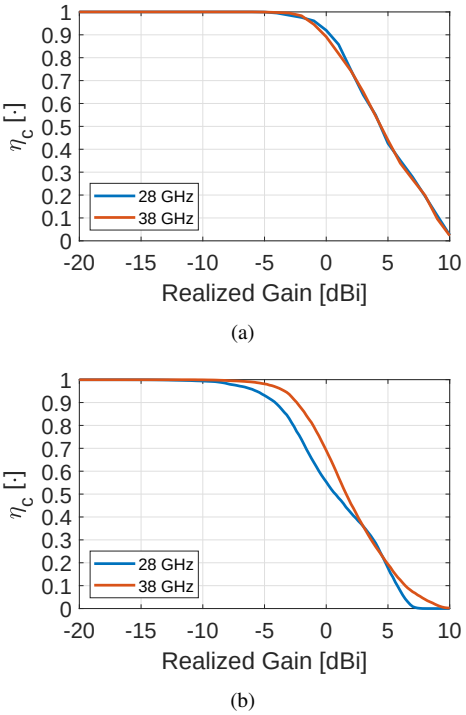

Fig. 19. (a) Simulated and (b) measured coverage efficiency characteristics of the antenna system for the analysed frequencies.

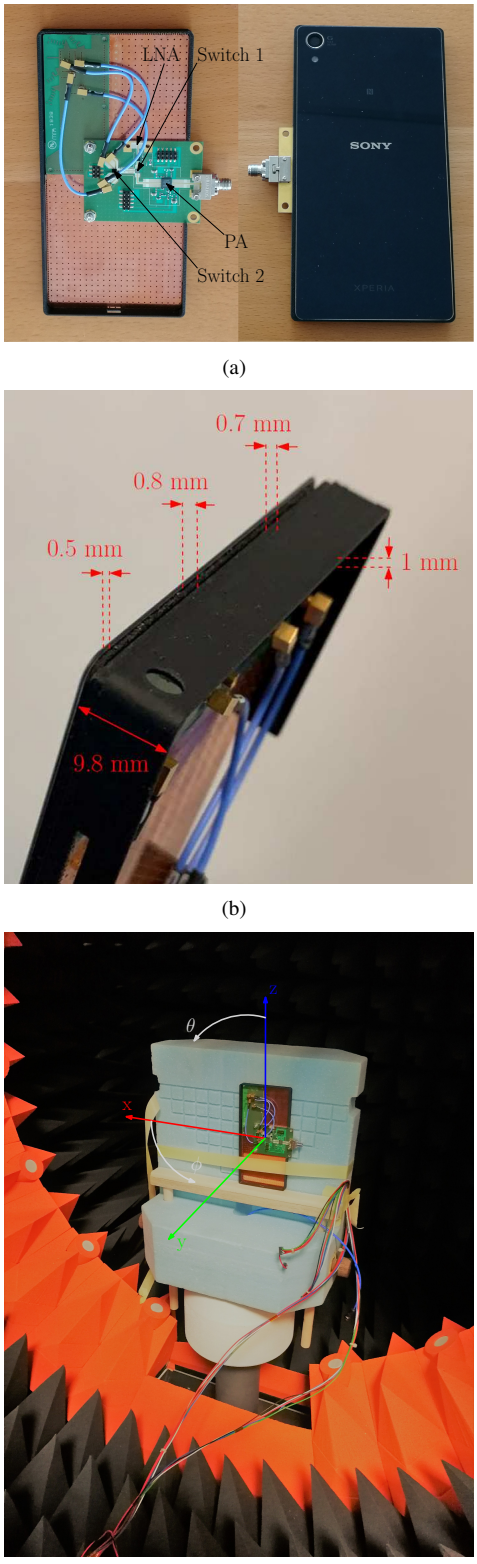

Fig. 20. (a) Yagi–Uda antenna array connected to the Sony FEM and mounted inside the Sony phone-case prototype, (b) dimensions of case and glass, and (c) active measurements setup in the MVG StarLab 50 GHz

when the display is positioned in $\phi = 0$, the EIRP drops to 0 dBm, as emerged also from the simulations results in Fig. 22(b). On the other hand, the undesired back radiation increases its power and enlarges its coverage.

Therefore, to further evaluate the influence of the phone-case and the glass on the antenna performance, the surface currents related to the first element are simulated with CST and plotted in Fig. 24 with the time average amplitude. Considering the effects of the phone-case on the antenna behaviour (Fig. 24(b)), it is possible to observe that the current generated

This article has been accepted for publication in a future issue of this journal, but has not been fully edited. Content may change prior to final publication. Citation information: DOI 10.1109/TAP.2019.2925189, IEEE Transactions on Antennas and Propagation

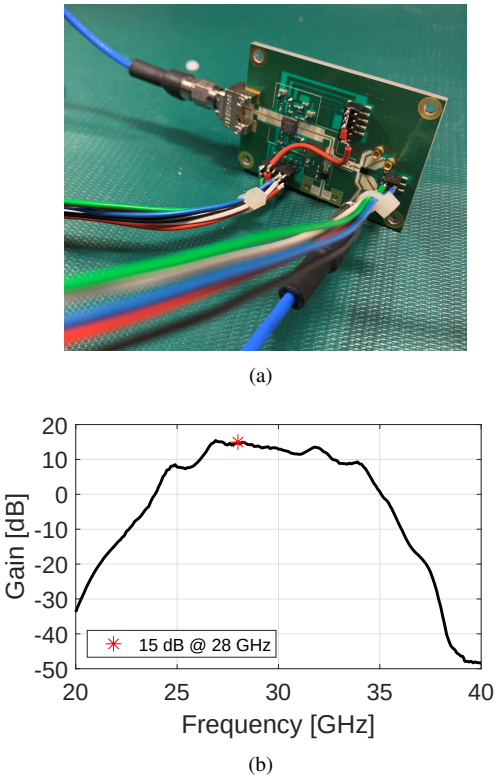

Fig. 21. (a) Measurement setup to test the gain performance of the FEM and (b) results in the band $20 - 40$ GHz.

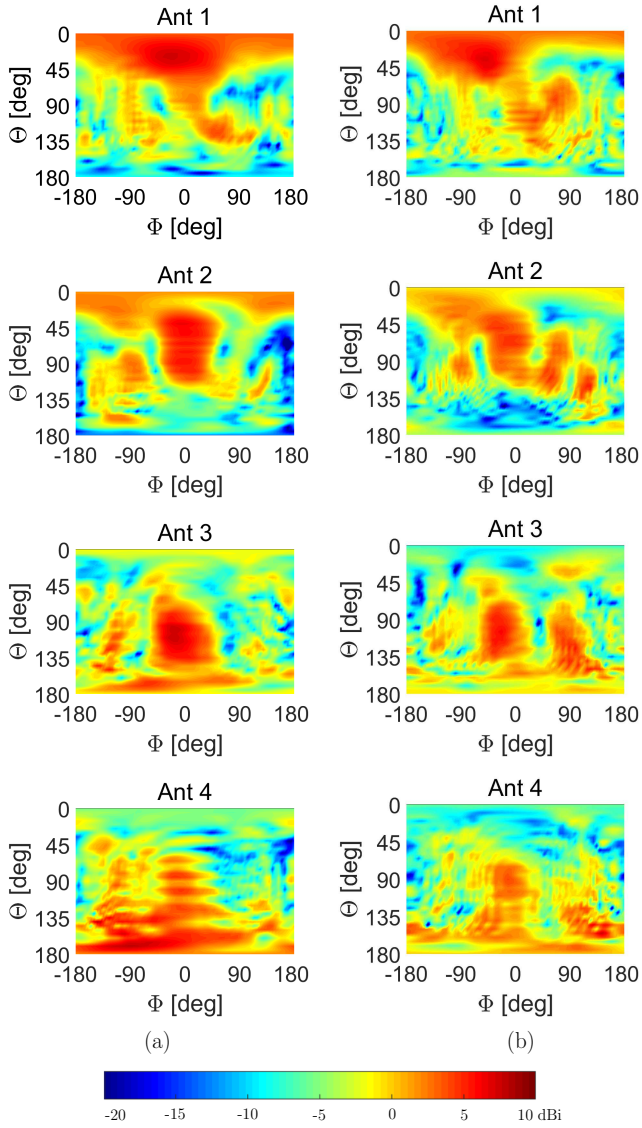

Fig. 22. Simulated radiation pattern at 28 GHz of the corner antenna array (a) inside the phone-case and (b) with the glass respectively. For ϕ varying from $-180°$ to $180°$ the corresponding value along θ varying from $0°$ to $180°$ has been plotted.

by antenna 1 is not only directed to the next antenna element, but it also flows down to the substrate. More significant is the impact of the glass, as visible in Fig. 24(c). In fact, due to its presence, the surface currents are also spread back to the ground plane and along its top and right edge.

Finally, simulations are carried out to analyse how a case made up of different material affects the radiation performance of the antenna array. In particular, the polycarbonate case used for the active measurements is compared to a ceramic and a metal frame. The radiation patterns of the first antenna element in the first two cases are very similar but, while with the polycarbonate frame the main beam reaches a maximum gain of 6.9 dBi (Fig. 25(a)), with ceramic it is possible to notice a lower gain of 6.1 dBi and a significant reflection of 5.9 dBi (Fig. 25(b)). Moreover, looking at the results in Fig. 25(c), it turns out that the metal frame totally alters the radiation characteristics of the antenna, reflecting the main beam with 7 dBi gain towards the bottom of the structure, while the desired area is covered with only 4.2 dBi. This metal blockage to the main beam generally happens to nearly all the horizontally-polarized antennas, and can efficiently be suppressed by the technique in [37].

VI. Conclusion

This work is focused on the investigation of an alternative design to solve the performance limitations of the phased antenna arrays. First goal to accomplish is the realization of a wideband component with large coverage and high gain over the whole frequency range. Therefore, it is necessary to eliminate any dependence of the frequency to the phase, so to find a different solution to allow beam steering without the need for phase shifters. The initial design consists of a switchable array of five high gain Quasi-Yagi antennas with different orientation, placed on the short edge of the mobile device PCB. Switching to the feed of each element, it is possible to scan an area of $180°$ with realized gain of 8 dBi on average at 28 and 38 GHz. The structure is then optimized, giving a compact corner array of four elements, which has been fabricated and then measured with the MVG Starlab 50 GHz. The passive measurements results are evaluated by considering the 3D-radiation pattern of the single elements and the TSP of the whole array. Despite a reduction of 2 dB in gain at the lower frequencies, the radiation properties of the realized prototype are confirmed. Moreover, active measurements of the array connected to the Sony switch and integrated in the phone-case lead to similar conclusions, the desired area is covered

This article has been accepted for publication in a future issue of this journal, but has not been fully edited. Content may change prior to final publication. Citation information: DOI 10.1109/TAP.2019.2925189, IEEE Transactions on Antennas and Propagation

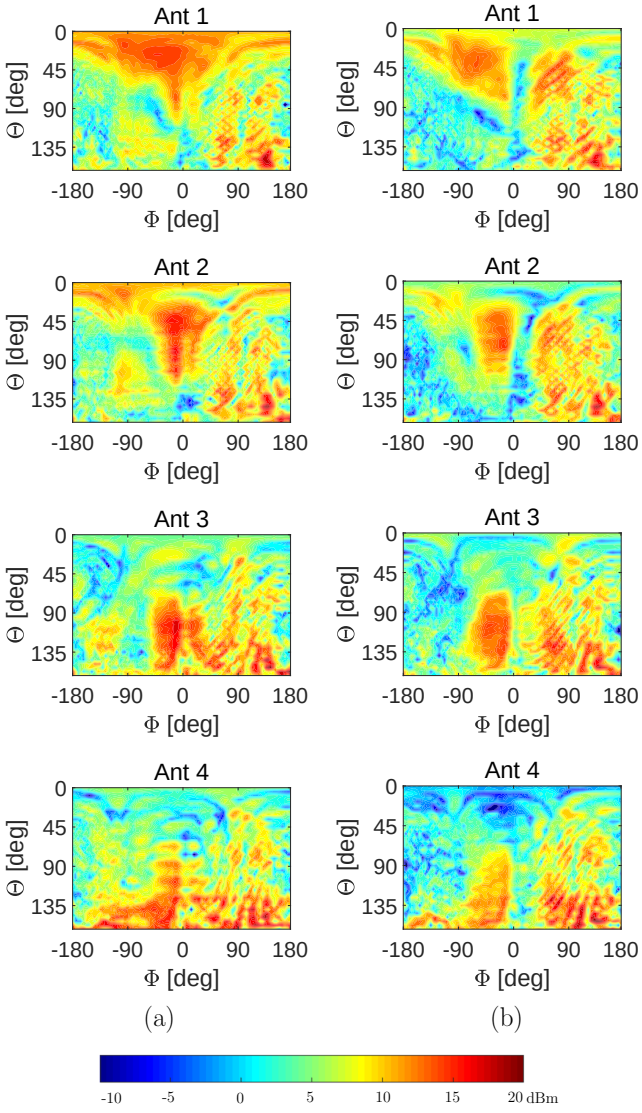

Fig. 23. Measured radiation pattern at 28 GHz of the corner antenna array (a) inside the phone-case and (b) with the glass respectively. For ϕ varying from -180° to 180° the corresponding value along θ varying from 0° to 162° has been plotted.

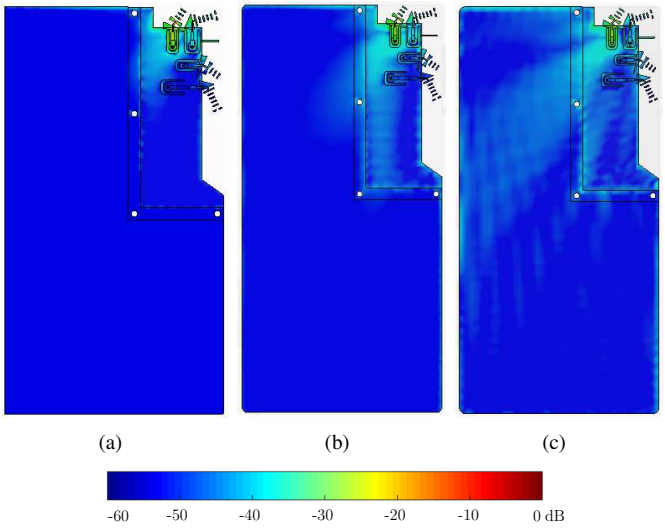

Fig. 24. Surface currents due to the first antenna element at 28 GHz (a) in free space, (b) when the array is mounted inside the phone-case only and (c) with the glass added.

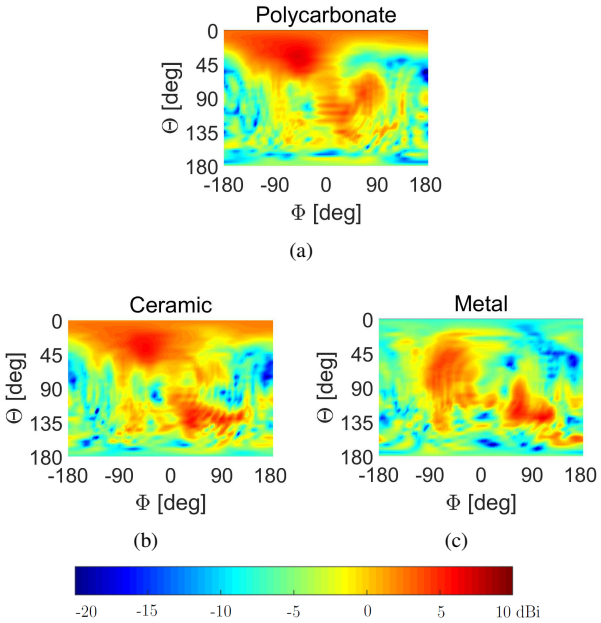

Fig. 25. Simulated 3D-radiation pattern of the first element at 28 GHz inside (a) polycarbonate, (b) ceramic and (c) metal case, to evaluate the impact of different frames on the antenna performance.

by simply switching to the feed of the corresponding antenna element. Future work requires careful consideration of the effects of the high permittivity components on the performance of the proposed antenna array. A further improvement consist in exploiting different kind of antennas in order to maximize the gain and reduce the width of the clearance to 5 mm, as required by the 5G mobile communication systems.

ACKNOWLEDGMENTS

The authors would like to thank the engineers Alessandro Scannavini, Lucia Scialacqua, Nicolas Gross and Romain Van Der Sypt from MVG for valuable assistance in the measurements setup and analysis and the PhD students Rocio Rodriguez Cano and Igor Syrytsin for precious help in the data processing. The work presented in this paper has been conducted under the framework of the RANGE project, supported by The Innovation Fund Denmark together with industry partners: WiSpry, AAC and Sony Mobile.

REFERENCES

[1] T. S. Rappaport, F. Gutierrez, E. Ben-Dor, J. N. Murdock, Y. Qiao, and J. I. Tamir, "Broadband millimeter-wave propagation measurements and models using adaptive-beam antennas for outdoor urban cellular communications," *IEEE Trans. Antennas Propag.*, vol. 61, no. 4, pp. 1850–1859, 2013.

[2] C. Narayan, *Antennas And Propagation*. Technical Publications, 2007.

[3] A. V. Alejos, M. G. Sanchez, and I. Cuinas, "Measurement and analysis of propagation mechanisms at 40 ghz: Viability of site shielding forced by obstacles," *IEEE Trans. Veh. Technol.*, vol. 57, no. 6, pp. 3369–3380, 2008.

[4] S. Rajagopal, S. Abu-Surra, Z. Pi, and F. Khan, "Antenna array design for multi-gbps mmwave mobile broadband communication," in *Global Telecommunications Conference (GLOBECOM)*. IEEE, 2011, pp. 1–6.

[5] L. Stark, "Microwave theory of phased-array antennas — a review," *Proceedings of the IEEE*, vol. 62, no. 12, pp. 1661–1701, 1974.

[6] R. C. Hansen, *Phased array antennas*. John Wiley & Sons, 2009, vol. 213.

[7] D. Parker and D. C. Zimmermann, "Phased arrays-part 1: theory and architectures," *IEEE Trans. Microw. Theory Tech.*, vol. 50, no. 3, pp. 678–687, 2002.

[8] K. Phalak and A. Sebak, "Aperture coupled microstrip patch antenna array for high gain at millimeter waves," in *International Conference on Communication, Networks and Satellite (COMNETSAT)*. IEEE, 2014, pp. 13–16.

[9] S. Zhang, X. Chen, I. Syrytsin, and G. F. Pedersen, "A planar switchable 3-d-coverage phased array antenna and its user effects for 28-ghz mobile terminal applications," *IEEE Trans. Antennas Propag.*, vol. 65, no. 12, pp. 6413–6421, 2017.

[10] W. Hong, K. Baek, Y. Lee, and Y. G. Kim, "Design and analysis of a low-profile 28 ghz beam steering antenna solution for future 5g cellular applications," in *MTT-S International Microwave Symposium (IMS)*. IEEE, 2014, pp. 1–4.

[11] N. Ojaroudiparchin, M. Shen, S. Zhang, and G. F. Pedersen, "A switchable 3-d-coverage-phased array antenna package for 5g mobile terminals," *IEEE Antennas Wireless Propag. Lett.*, vol. 15, pp. 1747–1750, 2016.

[12] H. Xia, J. Lei, L. Meng, and G. Yang, "Design and analysis of a compact reconfigurable phased antenna array with 3d coverage for 5g applications in portable devices," in *Progress in Electromagnetic Research Symposium (PIERS)*. IEEE, 2016, pp. 2459–2463.

[13] J. Bang, Y. Hong, and J. Choi, "Mm-wave phased array antenna for whole-metal-covered 5g mobile phone applications," in *2017 International Symposium on Antennas and Propagation (ISAP)*. IEEE, 2017, pp. 1–2.

[14] K. R. Mahmoud and A. M. Montaser, "Design of dual-band circularly polarised array antenna package for 5g mobile terminals with beam-steering capabilities," *IET Microwaves, Antennas & Propagation*, vol. 12, no. 1, pp. 29–39, 2017.

[15] Y.-W. Hsu, T.-C. Huang, H.-S. Lin, and Y.-C. Lin, "Dual-polarized quasi yagi–uda antennas with endfire radiation for millimeter-wave mimo terminals," *IEEE Trans. Antennas Propag.*, vol. 65, no. 12, pp. 6282–6289, 2017.

[16] B. Noori, M.-j. Tsai, B. W. Shiu, M. A. Mow, Y. Ouyang, M. Pascolini, and R. Caballero, "Electronic device with millimeter wave yagi antennas," Oct. 26 2017, uS Patent App. 15/138,684.

[17] C. Di Paola, S. Zhang, and G. F. Pedersen, "Hybrid high gain antenna systems, devices and methods," Jan. 5 2018, uS Patent App. 62/614,092.

[18] T.-C. Huang, Y.-W. Hsu, and Y.-C. Lin, "End-fire quasi-yagi antennas with pattern diversity on ltcc technology for 5g mobile communications," in *2016 IEEE International Symposium on Radio-Frequency Integration Technology (RFIT)*. IEEE, 2016, pp. 1–3.

[19] P. Liu, X. Zhu, X. Wang, and L. Tian, "A siw-based vivaldi array antenna for 5g wireless communication systems," in *2017 IEEE International Symposium on Antennas and Propagation & USNC/URSI National Radio Science Meeting*. IEEE, 2017, pp. 529–530.

[20] I. Syrytsin, S. Zhang, G. F. Pedersen, and A. S. Morris, "Compact quad-mode planar phased array with wideband for 5g mobile terminals," *IEEE Trans. Antennas Propag.*, vol. 66, no. 9, pp. 4648–4657, 2018.

[21] J.-W. Lian, Y.-L. Ban, Z. Chen, B. Fu, and C. Xiao, "Siw folded cassegrain lens for millimeter-wave multibeam application," *IEEE Antennas Wireless Propag. Lett.*, vol. 17, no. 4, pp. 583–586, 2018.

[22] Y. Cheng, W. Hong, and K. Wu, "Design of a substrate integrated waveguide modified r-kr lens for millimetre-wave application," *IET microwaves, antennas & propagation*, vol. 4, no. 4, pp. 484–491, 2010.

[23] K. Tekkouk, M. Ettorre, L. Le Coq, and R. Sauleau, "Multibeam siw slotted waveguide antenna system fed by a compact dual-layer rotman lens," *IEEE Trans. Antennas Propag.*, vol. 64, no. 2, pp. 504–514, 2016.

[24] Y. S. Zhang and W. Hong, "A millimeter-wave gain enhanced multi-beam antenna based on a coplanar cylindrical dielectric lens," *IEEE Trans. Antennas Propag.*, vol. 60, no. 7, pp. 3485–3488, 2012.

[25] J.-W. Lian, Y.-L. Ban, C. Xiao, and Z.-F. Yu, "Compact substrate-integrated 4× 8 butler matrix with sidelobe suppression for millimeter-wave multibeam application," *IEEE Antennas Wireless Propag. Lett.*, vol. 17, no. 5, pp. 928–932, 2018.

[26] Y. Cao, K.-S. Chin, W. Che, W. Yang, and E. S. Li, "A compact 38 ghz multibeam antenna array with multifolded butler matrix for 5g applications," *IEEE Antennas Wireless Propag. Lett.*, vol. 16, pp. 2996–2999, 2017.

[27] L.-H. Zhong, Y.-L. Ban, J.-W. Lian, Q.-L. Yang, J. Guo, and Z.-F. Yu, "Miniaturized siw multibeam antenna array fed by dual-layer 8× 8 butler matrix," *IEEE Antennas Wireless Propag. Lett.*, vol. 16, pp. 3018–3021, 2017.

[28] T. C. Cheston and J. Frank, "Array antennas," JOHNS HOPKINS UNIV LAUREL MD APPLIED PHYSICS LAB, Tech. Rep., 1968.

[29] R. J. Mailloux, *Phased array antenna handbook*. Artech House Boston, 2005, vol. 2.

[30] J. Huang and A. C. Densmore, "Microstrip yagi array antenna for mobile satellite vehicle application," *IEEE Trans. Antennas Propag.*, vol. 39, no. 7, pp. 1024–1030, 1991.

[31] S. Lim and H. Ling, "Design of a closely spaced, folded yagi antenna," *IEEE Antennas Wireless Propag. Lett.*, vol. 5, no. 1, pp. 302–305, 2006.

[32] L. Lu, K. Ma, F. Meng, and K. S. Yeo, "Design of a 60-ghz quasi-yagi antenna with novel ladder-like directors for gain and bandwidth enhancements," *IEEE Antennas Wireless Propag. Lett.*, vol. 15, pp. 682–685, 2016.

[33] K. Kiminami, A. Hirata, and T. Shiozawa, "Double-sided printed bow-tie antenna for uwb communications," *IEEE Antennas Wireless Propag. Lett.*, vol. 3, no. 1, pp. 152–153, 2004.

[34] H. Wang, Y. Chen, F. Liu, and X. Shi, "Wideband and compact quasi-yagi antenna with bowtie-shaped drivers," *Electronics Letters*, vol. 49, no. 20, pp. 1262–1264, 2013.

[35] E. T. 38.101-2, "Nr; user equipment (ue) radio transmission and reception; part 2: Range 2 standalone," no. version 15.4.0, Jan. 2019.

[36] J. Helander, K. Zhao, Z. Ying, and D. Sjöberg, "Performance analysis of millimeter-wave phased array antennas in cellular handsets," *IEEE Antennas Wireless Propag. Lett.*, vol. 15, pp. 504–507, 2016.

[37] R. Rodriguez-Cano, S. Zhang, K. Zhao, and G. F. Pedersen, "Reduction of main beam-blockage in an integrated 5g array with a metal-frame antenna," *IEEE Trans. Antennas Propag.*, vol. 67, no. 5, pp. 3161–3170, 2019.